Experimental and kinetic modeling studies on oxidation of n-heptane under oxygen enrichment in a jet-stirred reactor

Can Wang[1,], *Xin* Zhong[1], *Haifeng* Liu[1, *], *Tengda* Song[1], *Hu* Wang[1], *Bin* Yang[2] , and *Mingfa* Yao[1]

[1]State Key Laboratory of Engines, Tianjin University, Tianjin, 300072, China
[2]Center for Combustion Energy and Key Laboratory for Thermal Science and Power Engineering of MOE, Tsinghua, University, Beijing, 100084, China

Keywords: N-heptane, Kinetic, Oxygen enrichment, Jet-stirred reactor.

Abstract. Oxygen-enriched combustion can improve thermal efficiency and reduce CO, unburned hydrocarbons and soot emissions in internal combustion engines. There are significant differences in the combustion process and pollutant emissions between oxygen-enriched and air condition. In order to develop an improved understanding of the effect of oxygen concentration on n-heptane oxidation, the jet-stirred reactor oxidation characteristics of n-heptane were experimentally tested at temperatures of 450-950 K and pressures of 1.03 atm with the residence time (τ) of 2 s, under the condition of oxygen mole fractions from 0.055 to 0.6. Meantime, the simulations were performed on CHEMKIN. Results show that, firstly, with the increase of oxygen concentration, the NTC (Negative Temperature Coefficient) effect is weakened, mainly due to the strengthening of low-temperature reaction path, which is also the reason for the improvement of ignition stability in cold-start condition of engines. Secondly, the activity of the reaction system improves with the increase of oxygen concentration. Within 500-750 K, it is due to enhancement of the low-temperature reaction path. When the temperature is higher than 750 K, the improvement is due to the enhancement of decomposition of H2O2 and addition reaction of H and O2. Thirdly, with the increase of oxygen concentration, both the generation and consumption of CO are strengthened, which leads to the tip of the diesel spray flame changing from soot area under air condition to the CO chemiluminescence.

1 Introduction

The use of oxygen-enriched air offers advantages in many applications, such as internal combustion (IC) engines, metal heating and melting[1], glass melting, waste incineration, boiler and gas turbine of the power plant[2]. For IC engines, oxygen-enriched combustion can

---

* Corresponding author: haifengliu@tju.edu.cn

improve thermal efficiency and reduce CO, unburned hydrocarbons and soot emissions with higher NOx emissions[3, 4]. However, the study of Poola et al.[5] showed that NOx and other emissions could be reduced simultaneously through appropriate oxygen-fuel enrichment ratio (23%) and retard injection timing (by 7 degrees) in a locomotive diesel engine. Exhaust gas recirculation and water emulsified diesel technologies were also effective methods to control NOx emission in oxygen-enriched combustion[6, 7]. What's more, oxygen-enriched combustion can improve cycle fluctuation, cold start emission and insufficient power caused by thin air in plateau environments [8, 9].
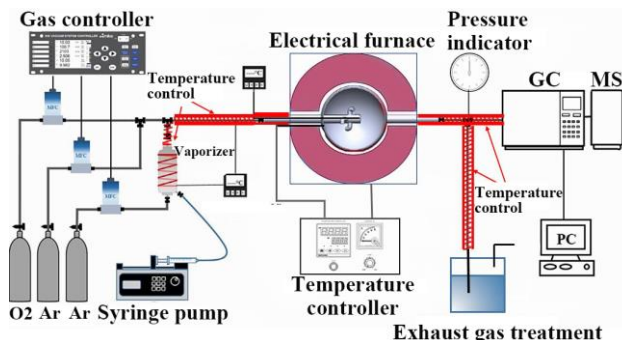
The development of oxygen separation technology from air provides the feasibility for oxygen-enriched combustion and attracts researchers to conduct further research on higher oxygen concentration levels. In 1998, Callaghan et al. [10] developed an oxygen-enriched membrane that could be applied to the engine. Rigby et al. [11] designed and optimized the combination of oxygen-enriched membrane/turbocharger, which could simplify the equipment and reduce the cost of oxygen-enriched preparation. Oxygen-enriched membrane modules with good performance have been developed rapidly, especially hollow fiber membrane, which has a good application prospect. At present, there have been successful experiences in applying oxygen-enriched membrane to engine at home and abroad[9, 12]. These studies show that the rapid development of on-line oxygen production technology provides a guarantee for oxygen-enriched combustion.

Some studies have shown that there are significant differences in the combustion process, NOx, CO, soot and other typical species under oxygen-enriched conditions and air conditions. Zheng et al.[13] studied polyoxymethylene dimethyl ethers spray flame at different oxygen levels in a constant volume vessel. Results showed that as the oxygen concentration increases, the flame natural luminosity and propagation speed increased, the position of lift-off region and flame tip moved towards the injector nozzle, and the flame width became narrower. Wu et al. [14] studied the effect of oxygen content on n-heptane auto-ignition characteristics in a HCCI engine. They argued that the higher oxygen content also improved the H-atom abstraction, first O2 addition, second O2 addition and peroxyalkylhydroperoxide isomerization, thereby improving the overall reaction rate and the heat release fraction of low-temperature reactions. The experiments of Nidhi et al.[15] on a spark-ignition engine showed that NOx emission decreased drastically with 60.4% oxygen and it was lower than base oxygen (21%) because of decrease in nitrogen content in the inducted air, which showed the potential of oxygen-enriched combustion to improve the trade-off relationship between NOx and soot.

As a primary reference fuel of diesel fuel, the mechanisms of n-heptane oxidation were well studied. However, in the mechanism studies of n-heptane, the equivalence ratios were mostly between 0.1-3[16-19], and the effect of oxygen concentration on n-heptane oxidation is little systematically studied under a wide range of oxygen concentration conditions.

The objective of the present study is to develop an improved understanding of the effect of oxygen concentration on n-heptane oxidation under oxygen enrichment conditions using a combination of experiments and modeling. On one hand, the results will help to expand the experimental database of n-heptane mechanisms in a wide range of oxygen concentrations. On the other hand, it is conducive to the application of oxygen-enriched combustion technology.

2 Experimental setup

Fig. 1. Schematic for JSR experimental setup.

Table 1. The initial species compositions and equivalence ratios.

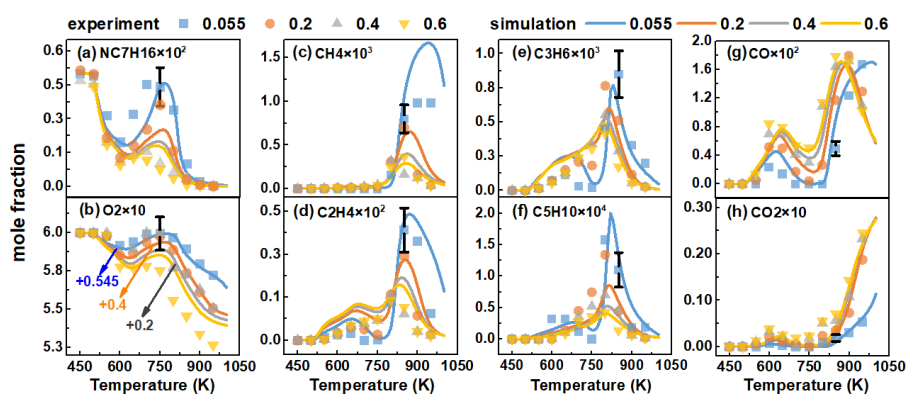| NC7H16	O2	AR	Equivalence ratio
	Mole fraction		
0.005	0.055	0.94	1
0.005	0.2	0.795	0.25
0.005	0.4	0.595	0.125
0.005	0.6	0.395	0.08

Fig. 1 shows the schematic of experimental setup. Briefly, the experimental platform consists of a jet-stirred reactor (JSR), a fuel injection system, a gas supply system, a temperature control system, and a species detection equipment. The JSR used in the experiment was provided by University of Science and Technology of China and details about it can be found in literature[20]. Some modifications had been made to remove the quartz nozzle in order to adapt to the current detection equipment GC-MS/FID. The JSR was made of fused silica with a volume of $103\pm1cm^3$ and was heated by an electrical furnace. The internal pressure of JSR is maintained at atmospheric pressure and measured in real time by a pressure gauge with an accuracy of 1%. Thermocouples were placed in the center and outside of the JSR to monitor its temperature difference. Argon with a purity of 99.999% was used to dilute the fuel. The gas flow was regulated and monitored by MKS controller. The mixture passed through a preheating zone (about 60 cm in length) to reduce temperature gradient inside the reactor. The fuel NC7H16 was injected into the vaporizer through a micro syringe pump. The temperature in the vaporizer was heated to about 20 K above the boiling point of the fuel by the temperature control device. The evaporated fuel was carried out of the vaporizer by a constant argon flow of 100 sccm. The temperatures were measured by a K-type thermocouple with around ±2 K accuracy. The pressure of gas mixture inside the reactor was kept at near 1.03 atm and a pressure sensor was installed at the exhaust port to monitor the pressure in the reactor during the experiment. HP-Plot Q column was used for species separation, and Flame Ionization Detector (FID) and Thermal Conductivity Detector (TCD) were used for quantification of species.

The n-heptane oxidation experiments were performed at 450-950 K with the residence times of 2 s. The initial species compositions and equivalence ratios are shown in Table 1. The concentrations of methane, ethylene, propylene and n-heptane were quantified by FID, and oxygen, carbon monoxide and carbon dioxide were quantified by TCD. The effective carbon number (ECN) method was applied in the mole fraction calculations of pentene. Accuracy is mainly affected by the measurement precision of peak areas, fuel injection

system, the stability of column and ECN method. For most species, the uncertainties in measured mole fractions were within ± 20%. While for pentene, the uncertainty was estimated at ± 30% due to the application of the ECN method.

3 Kinetic modeling

In this work, simulations of n-heptane oxidation were performed using the Perfectly Stirred Reactor (PSR) Code in CHEMKIN. The detailed mechanism [21] of n-heptane (version 3.1) from Lawrence Livermore National Laboratory (LLNL) was adopted. The mechanism was based on the previously developed and very successful mechanism of Curran et al.[22], and has been validated extensively. Over the series of experiments numerically investigated, the initial pressure ranged from 3 to 50 atm, the temperature from 650 to 1200 K, and equivalence ratios from 0.3 to 1.0. The mechanism performs well at both low and high temperatures and over a broad pressure range. Fig. 2 shows mole fractions of important species in experiments and simulations. In order to reflect the changes in oxygen concentrations more clearly, oxygen mole fractions were increased by 0.545, 0.4, and 0.2 under the oxygen concentrations of 0.055, 0.2, and 0.4 in Fig. 2b, respectively. The results of simulation reproduced the mole fractions of fuel and key intermediate species well, which indicated the existing mechanism was reliable under oxygen-enriched conditions. Therefore, the mechanism was not further improved in this paper, but more chemical kinetics analysis on oxygen-enriched conditions was carried out to further reveal the experimental results.

Fig. 2. Comparisons of mole fractions of important species in experiments and simulations under different oxygen concentrations.
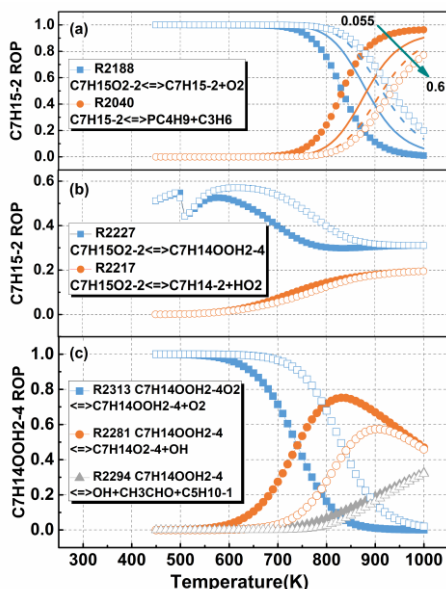
4 Results and discussion

4.1 The oxidation of n-heptane

As can be seen from Fig. 2a, oxygen concentration has little influence on n-heptane mole fraction under low temperature (<600 K) and high temperature (>900 K). When the temperature is in the range of 600-900 K, the mole fraction of n-heptane increases with the increase of temperature due to the NTC (Negative Temperature Coefficient) effect. The mole fraction of n-heptane decreases as oxygen concentration increases, indicating that the increasement of oxygen concentration weakens the NTC effect.

In order to further explore the influence of oxygen concentration on NTC behavior, the reactions with higher rates of production (ROPs) were selected to analyze the competition

between high-temperature path and low-temperature path. The relative ROPs of C7H15-2, C7H15O2-2 and C7H14OOH2-4 are shown in Fig. 3. As can be seen from Fig. 3a, the relative ROPs gaps of each reaction narrow with increasing oxygen concentration. Therefore, only the relative ROPs of oxygen concentrations of 0.055 (solid) and 0.6 (hollow) are shown in Fig. 3b and 3c for the neatness of the figures. As seen in Fig. 3, the low temperature reactions (R2188, R2227 and R2313) are strengthened with the increase of oxygen concentration, while the contribution proportions of high temperature reaction (R2040 and R2281) decrease. Besides, the contribution proportions of R2217 and R2294 in the high temperature reaction path are not affected by oxygen concentration. With the increase of oxygen concentration, the enhancement of the second O2 addition reaction accelerates the consumption of C7H14OOH2-4 and promotes the forward equilibrium of the isomerization reaction R2227, so the relative ROP of R2227 increases.

Fig. 3. The contribution proportions of low-temperature and high-temperature reactions in the consumption paths of C7H15-2, C7H15O2-2 and C7H14OOH2-4. (Solid shape, solid line, dotted line, hollow shape represent oxygen concentrations of 0.055, 0.2, 0.4 and 0.6, respectively.)

Under different oxygen concentrations, the competitive ratios of low-temperature path and high-temperature path vary in amplitude and temperature range. The influence of O2 on isomerization reaction is relatively small, while it has a great effect on the first O2 addition reaction and the second O2 addition reaction. With the increase of oxygen concentration, the enhancement of isomerization reaction and the second O2 addition reaction begins at about 600 K, while the enhancement of the first O2 addition reaction begins at about 750 K. Therefore, within 600-750 K, the NTC effect is weakened with the increase of oxygen concentration, which is mainly attributed to the enhancement of isomerization reaction R2227 and the second O2 addition reaction R2313. In the range of 750-900 K, with the increase of oxygen concentration, the strengthening of the above low-temperature reactions all contributes to the weakening of NTC effect, of which R2188 and R2313 contribute more.
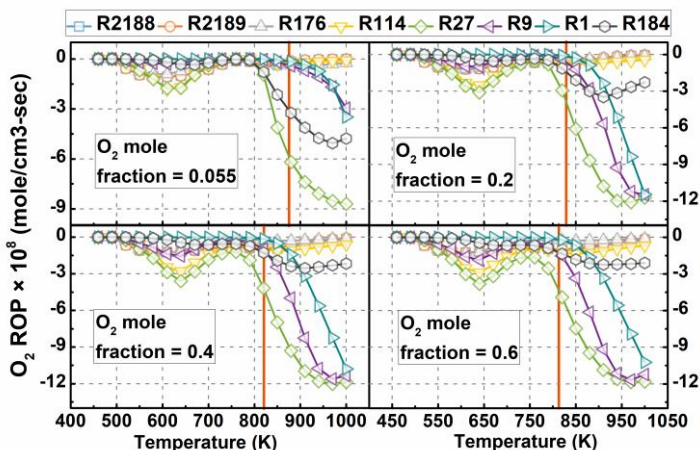
4.2 The consumption of oxygen

As can be seen from Fig. 2b, the oxygen consumption rate increases with the increase of oxygen concentration. Especially when the temperature is 750 K, the oxygen consumption

rate is almost zero at 0.055 oxygen concentration, while it increases obviously at high oxygen concentration. In order to explore which reactions are greatly affected by the increase of O2 concentration, the absolute ROPs of O2 consumption reactions were analyzed, which are shown in Fig. 4. The reactions involved are listed in the Table 2. The actual ROPs values were multiplied by 10^8 for brevity of the axis labels in the figures.

Table 2. Reactions with higher absolute values of ROPs.

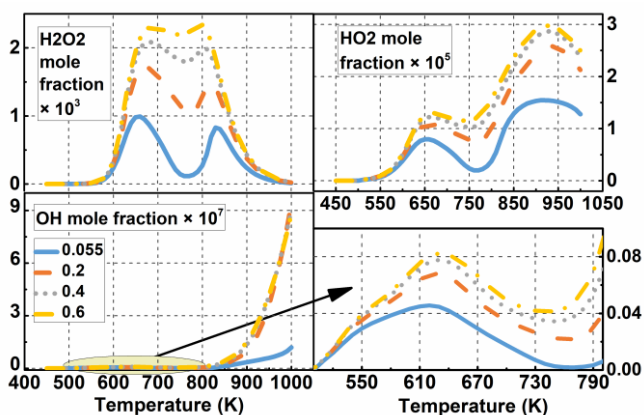| Number	Reactions
R2188	C7H15O2-2<=>C7H15-2+O2
R2189	C7H15O2-3<=>C7H15-3+O2
R176	C2H5O2<=>C2H5+O2
R114	CH3+O2(+M)<=>CH3O2(+M)
R27	HCO+O2<=>CO+HO2
R9	H+O2(+M)<=>HO2(+M)
R1	H+O2<=>O+OH
R184	C2H5+O2<=>C2H4+HO2

R27 always occupies a large proportion of the O2 consumption reactions. In the range of 500-750 K, addition reactions (R114, R176, R2188 and R2189) between alkyl and O2 also account for a large proportion. When the oxygen concentration increases from 0.055 to 0.2, the ROPs of R27 and R114 increase greatly. With the further increase of oxygen concentration, the increasing trend slows down. In the temperature range of 750-800 K, when oxygen concentration is 0.055, the rate of O2 consumption reaction is almost zero. However, with the increase of O2 concentration, the O2 consumption rate increases due to the enhancement of R27 and the addition reactions of the alkyl group with O2. Within 800-1000 K, the consumption reactions of O2 mainly include R27, R1, R9 and R184. When the oxygen concentration increases from 0.055 to 0.2, the ROPs of R1 and R9 increase greatly, while the ROP of R184 decreases. When the oxygen concentration increases from 0.2 to 0.6, there are few changes in the peak ROPs of R27, R1 and R9, but the increase of R9 ROP with oxygen concentration of 0.2 occurs at lower temperature. The ROP of R184 decreases slightly with the increase of oxygen concentration.
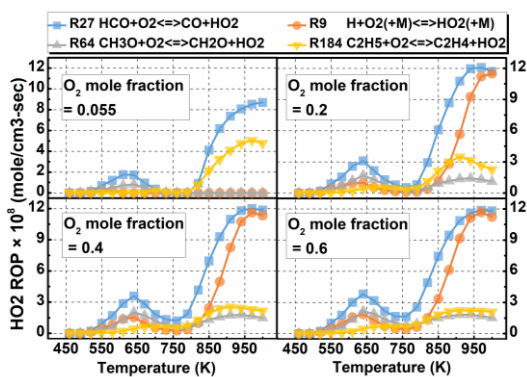

Fig. 4. The absolute ROPs of O2 consumption reactions.
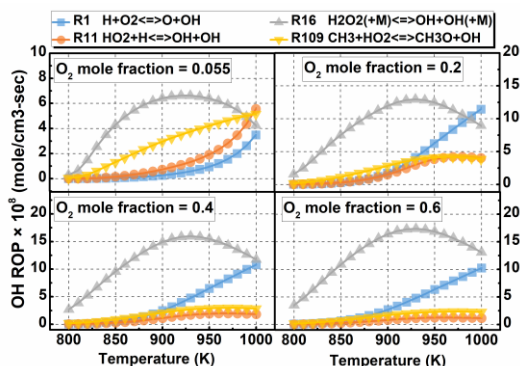
4.3 The formation of key intermediate products

Fig. 5 shows the mole fractions of H2O2, HO2 and OH under different temperatures and oxygen concentrations. With the increase of O2 concentration, the concentrations of H2O2, HO2 and OH increase, but the growths slow down. The main source of H2O2 is HO2+HO2=H2O2+O2, so the concentration of HO2 has an important influence on the concentration of H2O2. Fig. 6 shows the absolute ROPs of the reactions with high ROPs to produce HO2, and the ROPs values were multiplied by 10^8. R27 plays a dominant role in the production of HO2 under different temperatures and O2 concentrations, and the ROP of it increases with the increasement of oxygen concentration. Besides, when the oxygen concentration is 0.055, R184 makes a greater contribution to the formation of HO2, while the contribution proportions of R9 increase significantly at high oxygen concentration. Finally, the concentrations of HO2 and H2O2 increase with the increase of oxygen concentration.

Fig. 5. The mole fractions of H2O2, HO2 and OH at different temperatures and oxygen concentrations.

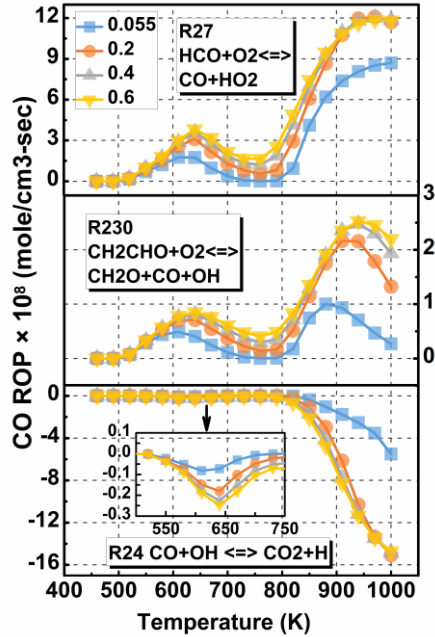**Fig. 6.** The absolute ROPs of the reactions to produce HO2.

Fig. 7. The absolute ROPs of the reactions of generating OH.

As the above analysis of n-heptane oxidation, the increase of O2 concentration promotes low-temperature reaction paths, thus promoting the formation of OH. In the temperature range of 500-750 K, R2331 (C7H14OOH2-4O2<=>NC7KET24+OH) and R2337 (C7H14OOH3-5O2<=>NC7KET35+OH) contribute a large proportion to the formation of OH. Within 800-1000 K, the reactions with higher ROPs among the reactions of generating OH were analyzed, and the absolute ROPs are shown in Fig. 7. The main source of OH is the decomposition of H2O2. With the increase of oxygen concentration, H2O2 concentration increases, and thus the decomposition rate of H2O2 to produce OH also increases. At 1000 K, when the oxygen concentration is 0.055, the contribution ratios of R1, R11, R16 and R109 to the generation of OH are close. However, with the increase of oxygen concentration, the main reactions to produce OH become R16 and R1, and the contribution ratio of R16 increases with the increase of oxygen concentration.

In conclusion, within 500-750 K, O2 improves the reactivity of the reaction system by promoting the low temperature reaction path. When the temperature is higher than 750 K, the improvement of the activity is due to the increasing concentration of active radicals such as OH and HO2 which are mainly generated through R1, R9 and R16.
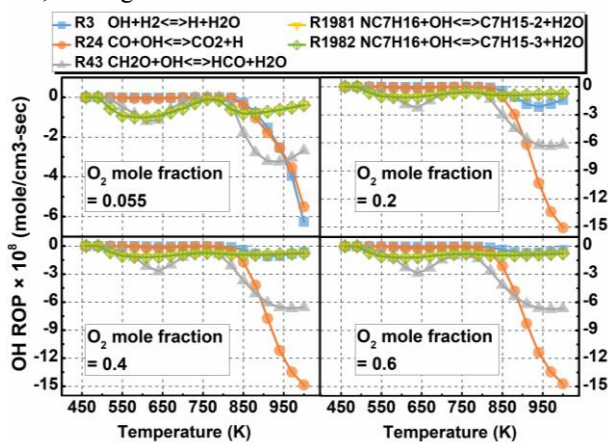
4.4 The formation and oxidation of CO

The analysis of O2 consumption reactions indicates the importance of O2 to CO. Therefore, the effect of O2 on CO was deeply discussed. As can be seen from Fig. 2g, the CO mole fraction shows double peaks with increasing temperature. When the oxygen concentration is within 0.2-0.6, the peaks of CO mole fraction appear at about 640 K and 870-890 K, while it appears at about 625 K and 985 K at oxygen concentration of 0.055. When the temperature is lower than 870 K, the mole fraction of CO increases with the increase of oxygen concentration. As temperature increases further, the CO mole fractions of oxygen concentrations of 0.2-0.6 decrease rapidly, and there are no significant differences among them. However, when the oxygen concentration is 0.055, the CO mole fraction continues to increase with the increase of temperature until 990 K. The CO mole fraction under oxygen concentration of 0.055 is significantly higher than that under higher oxygen concentration at 1000 K.

Fig. 8. The absolute ROPs of CO.

In order to explore the change rules of CO under different oxygen concentrations and temperatures, the formation and consumption reactions of CO were analyzed. Fig. 8 shows the absolute ROPs of CO. R27 and R230 are the main CO formation reactions. In CO consumption reactions, R24 contributes more than 75% under different temperatures and O_2 concentrations. On one hand, CO is mainly oxidized by OH. On the other hand, OH also promotes the formation of HCO ($CH_2O+OH<=>HCO+H_2O$), thus promoting the formation of CO through R27. Therefore, the consumption reactions ROPs of OH were additionally analyzed, which were shown in Fig.9. The oxidation of CO (R24) and the formation of HCO (R43) account for a large proportion of OH consumption, especially when the temperature is higher than 800 K. When the oxygen concentration is 0.055, the proportion of R3 in OH consumption reactions is significantly higher than that under high oxygen concentration, which consumes OH, leading to slower rates of CO oxidation and formation.
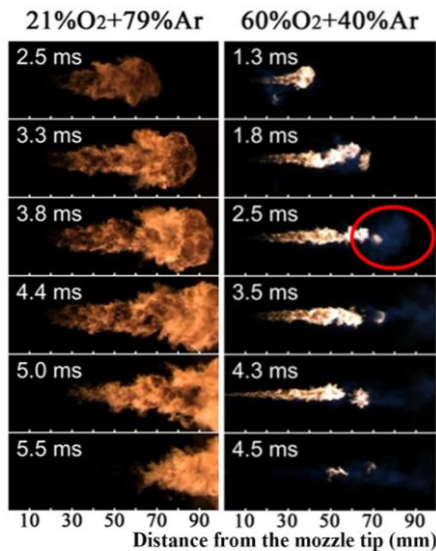

Fig. 9. The absolute ROPs of the reactions of consuming OH.

In the temperature range of 500-750 K, with the increase of oxygen concentration, both the formation rate and consumption rate of CO increase, but the formation rate is much higher than the consumption rate, leading to higher CO mole fraction. When the temperature is greater than 800 K, the rate of CO oxidation reaction (R24) begins to increase rapidly. At about 870 K, CO mole fraction reaches peak at high oxygen concentration, since the rates of CO formation and oxidation achieve a balance. As the temperature rises further, the reaction rate of R27 grows more and more slowly, and that of R230 even declines, while the rate of R24 increases rapidly, leading to the decrease of CO mole fraction. However, when the oxygen concentration is 0.055, the growth rate of CO oxidation reaction is slow. At about 990 K, the balance between CO generation and oxidation is achieved, and thus the mole fraction of CO reaches the peak.

4.5 The chemical reaction path analysis

The above analysis is conducive to further revealing the macroscopic differences between oxygen enrichment and air conditions shown in the experimental results of some studies, which has guiding significance for the application of oxygen-enriched combustion.
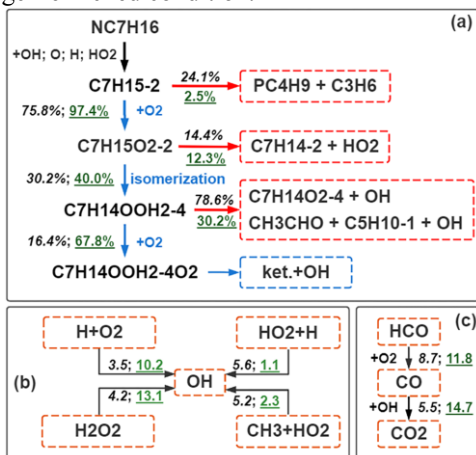
Fig. 10 shows the diesel spray in air and oxygen-enriched conditions, which was studied by Wang et al.[23] in an optical constant volume vessel. It has been found that with the rising of oxygen level, the ignition delay was shortened, the luminosity intensity in the flame core increased and the shape of the spray flame was shortened and narrowed. In addition to the reason that higher oxygen concentration allowed more fuels to reach the appropriate equivalent ratio more quickly, chemical kinetics also played an important role, which can be proved by the study on oxygen-containing fuel polyoxymethylene dimethyl ethers (PODE) by Zheng et al [13]. They conducted optical investigation on PODE spray flame at different oxygen levels in a constant volume vessel and obtained similar conclusions in the ignition delay, the luminosity intensity in the flame core and the shape of the spray flame.

Fig. 10. Single-shot, true-color natural flame luminosity images for different oxygen level of 21% and 60%, in the ambient temperature of 800 K and pressure of 4 MPa conditions[23].

Fig. 11a shows the reaction paths of n-heptane under oxygen concentrations of 0.055 and 0.6 at 800 K. The blue arrows represent low-temperature path, and the red arrows represent

high-temperature path. The data in the figure are the relative ROPs. Oxygen enrichment promotes the low temperature reaction path including isomerization reactions and O2 addition reactions. Therefore, it promotes the decomposition of peroxyalkylhydroperoxide (e.g. C7H14OOH2-4O2), releasing OH and forming different ketohydroperoxide (ket.) species. The subsequent decomposition of ket. molecules leads to the formation of a carbonyl radical and another OH radical, which promotes chain branching, while the pyrolysis reaction path is endothermic. The enhancement of low temperature reaction path is one of the important reasons of the shortening of ignition delay and the improvement of cold start performance under oxygen-enriched condition.

Fig. 11. Chemical reaction path analysis (black italics: oxygen concentration of 0.055, green underline: oxygen concentration of 0.6.)

Fig. 11b shows the OH generation path under oxygen concentrations of 0.055 and 0.6 at 1000 K. The data in the figure are absolute ROPs multiplied by 10^8. Under high oxygen concentration, the formation rate of OH is significantly increased, which promotes large amounts of heat release and fuel oxidation. So the combustion speed was faster and luminosity intensity in the flame core increased under oxygen enrichment in the study [23].

The blue region caused by CO luminescence in the tip of the spray flame at high oxygen level is worth special attention. Fig. 11c shows the paths of CO generation and consumption under oxygen concentrations of 0.055 and 0.6 at 1000 K. The data in the figure are absolute ROPs multiplied by 10^8. Under oxygen-enriched conditions, the formation rates of both CO and OH are higher, leading to the enhancement of R24 (CO+OH<=>CO2+H). The increase of oxygen concentration reduced the soot, while the generation and oxidation of CO were enhanced, so that the blue areas appeared in the tip of the spray flame at high oxygen level instead of the soot areas under air conditions.

5 Conclusions

The jet-stirred reactor oxidation characteristics of n-heptane were studied at temperatures of 450-950 K and pressures of 1.03 atm with the residence time (τ) of 2 s, under the condition of oxygen mole fractions from 0.055 to 0.6. The simulations were performed on CHEMKIN with the detailed n-heptane mechanism from LLNL. The simulation results reproduced the mole fractions of fuel and key intermediate species well and the ROPs of important species were analyzed. The main conclusions based on both experiments and chemical kinetics are as follows:

1. With the increase of oxygen concentration, the NTC effect is weakened, mainly due to the strengthening of low-temperature reaction path. Within 600-750 K, weakened NTC effect is mainly attributed to the enhancement of isomerization reaction R2227 (C7H15O2-2<=>C7H14OOH2-4) and the second O2 addition reaction R2313 (C7H14OOH2-4O2<=>C7H14OOH2-4+O2). In the range of 750-900 K, R2188 (C7H15O2-2<=>C7H15-2+O2) and R2313 contribute more to weakened NTC effect. The enhancement of low-temperature path increases OH concentration, thus shortening ignition delay and improving the ignition stability in low temperature environment such as cold start condition of engines.

2. With the increase of oxygen concentration, the activity of the reaction system improves. Within 500-750 K, the improvement is due to enhancement of the low-temperature reaction path, which promotes the generation of OH. When the temperature is higher than 750 K, the improvement is due to the increasing concentration of active radicals such as OH and HO2 which are mainly generated through decomposition of H2O2 and addition reaction of H and O2. The increase of OH improves the reaction rates and leads to brighter and narrower diesel spray flame structures.

3. When temperature is lower than 870 K, CO mole fraction increases with oxygen concentration. It's because R27 (HCO+O2<=>CO+HO2) promotes the formation of CO and the oxidation rate of CO is very low. When the temperature is higher than 870 K, CO mole fractions of high oxygen concentrations decrease rapidly due to increased CO oxidation rate, while CO mole fraction of 0.055 oxygen concentration is still high. With the increase of oxygen concentration, both the generation and consumption of CO are strengthened, which leads to the tip of the diesel spray flame changing from soot area under air condition to the CO chemiluminescence area under oxygen-enriched conditions.

References

1. ZHANG X, TONG L, WANG L, et al. The application and analysis of the oxygen-enriched combustion [J]. Energy for Metallurgical Industry, 2007, (06): 41-4+60.

2. LI S Y, XU M X, JIA L F, et al. Influence of operating parameters on N2O emission in O-2/CO2 combustion with high oxygen concentration in circulating fluidized bed [J]. Applied Energy, 2016, 173: 197-209.

3. JEEVAHAN J, POOVANNAN A, SRIRAM V, et al. Effect of intake air oxygen enrichment for improving engine performance and emissions control in diesel engine [J]. International Journal of Ambient Energy, 2017, 40(1): 96-100.

4. BASKAR P, SENTHILKUMAR A. Effects of oxygen enriched combustion on pollution and performance characteristics of a diesel engine [J]. Engineering Science and Technology, an International Journal, 2016, 19(1): 438-43.

5. POOLA R B, SEKAR R. Reduction of NOx and Particulate Emissions by Using Oxygen-Enriched Combustion Air in a Locomotive Diesel Engine [J]. Journal of Engineering for Gas Turbines and Power, 2003, 125(2): 524-33.

6. ZHANG W, CHEN Z, LI W, et al. Influence of EGR and oxygen-enriched air on diesel engine NO–Smoke emission and combustion characteristic [J]. Applied Energy, 2013, 107: 304-14.

7. MELLO J P, MELLOR A M. NOx Emissions from Direct Injection Diesel Engines with Water/Steam Dilution [J]. SAE TECHNICAL PAPER SERIES, 1999, 1999-01-0836.

8. XIAO G F, QIAO X Q, HUANG Z, et al. Improvement of startability of direct-injection diesel engines by oxygen-enriched intake air [J]. Proceedings of the Institution of Mechanical Engineers, Part D: Journal of Automobile Engineering, 2007, 221(11): 1453-65.

9. ZHANG Y, XIONG Y, LIU X, et al. Operating performance of oxygen-enriched membrane module based on application to vehicle engine on highland [J]. Journal of Logistical Engineering University, 2010, 26(5): 51-5.

10. CALLAGHAN K, NEMSER S, POOLA R B, et al. Variable Air Composition with Polymer Membrane - A New Low Emissions Tool [Z]. SAE International. 1998. https://doi.org/ 10.4271/980178

11. RIGBY G R, WATSON H C. Application of Membrane Gas Separation to Oxygen Enrichment of Diesel-Engines [J]. Journal of Membrane Science, 1994, 87(1-2): 159-69.

12. YELVINGTON P E, ROTH R P, MAYO R E, et al. Oxygen-Enriched Combustion for Industrial Diesel Engines [J]. Proceedings of the Asme Internal Combustion Engine Division Fall Technical Conference, 2016, 1(V001T03A012).

13. ZHENG Z, LIU W, LIU H, et al. Optical investigation on polyoxymethylene dimethyl ethers spray flame at different oxygen levels in a constant volume vessel [J]. Science China Technological Sciences, 2021, 64(8): 1611-23.

14. WU Z, KANG Z, DENG J, et al. Effect of oxygen content on n-heptane auto-ignition characteristics in a HCCI engine [J]. Applied Energy, 2016, 184: 594-604.

15. NIDHI, SUBRAMANIAN K A. Experimental investigation on effects of oxygen enriched air on performance, combustion and emission characteristics of a methanol fuelled spark ignition engine [J]. Applied Thermal Engineering, 2019, 147: 501-8.

16. HERBINET O, HUSSON B, SERINYEL Z, et al. Experimental and modeling investigation of the low-temperature oxidation of n-heptane [J]. Combustion and Flame, 2012, 159(12): 3455-71.

17. KARWAT D M A, WAGNON S W, WOOLDRIDGE M S, et al. Low-temperature speciation and chemical kinetic studies of n-heptane [J]. Combustion and Flame, 2013, 160(12): 2693-706.

18. PELUCCHI M, BISSOLI M, CAVALLOTTI C, et al. Improved Kinetic Model of the Low-Temperature Oxidation of n-Heptane [J]. Energy & Fuels, 2014, 28(11): 7178-93.

19. SEIDEL L, MOSHAMMER K, WANG X X, et al. Comprehensive kinetic modeling and experimental study of a fuel-rich, premixed n-heptane flame [J]. Combustion and Flame, 2015, 162(5): 2045-58.

20. ZHOU Z Y, DU X W, YANG J Z, et al. The vacuum ultraviolet beamline/endstations at NSRL dedicated to combustion research [J]. J Synchrotron Radiat, 2016, 23: 1035-45.

21. MEHL M, PITZ W J, WESTBROOK C K, et al. Kinetic modeling of gasoline surrogate components and mixtures under engine conditions [J]. Proceedings of the Combustion Institute, 2011, 33: 193-200.

22. CURRAN H J, GAFFURI P, PITZ W J, et al. A comprehensive modeling study of n-heptane oxidation [J]. Combustion and Flame, 1998, 114(1-2): 149-77.

23. WANG Y, FENG L, GENG C, et al. Natural Flame Luminosity and Emission Spectra of Diesel Spray Flame under Oxygen-Enriched Condition in an Optical Constant Volume Vessel [J]. SAE Technical Paper Series. 2018.10.4271/2018-01-1781